ISSN 0001-4338, Izvestiya, Atmospheric and Oceanic Physics, 2012, Vol. 48, No. 1, pp. 47–56. © Pleiades Publishing, Ltd., 2012.
Original Russian Text © I.I. Mokhov, D.A. Smirnov, P.I. Nakonechny, S.S. Kozlenko, J. Kurths, 2012, published in Izvestiya AN. Fizika Atmosfery i Okeana, 2012, Vol. 48, No. 1, pp. 56–66.

Relationship between El-Niño/Southern Oscillation and the Indian Monsoon

I. I. Mokhov[a], D. A. Smirnov[b], P. I. Nakonechny[b], S. S. Kozlenko[a], and J. Kurths[c]

[a] *Obukhov Institute of Atmospheric Physics, Russian Academy of Sciences, Pyzhevskii 3, Moscow, 119017 Russia*
e-mail: mokhov@ifaran.ru

[b] *Saratov Branch, Kotel'nikov Institute of Radio Engineering and Electronics, Russian Academy of Sciences, ul. Zelenaya 38, Saratov, 410019 Russia*
e-mail: smirnovda@yandex.ru

[c] *Potsdam Institute for Climate Impact Research, D 14412 Potsdam, 601203 Germany*
e-mail: kurths@pik-potsdam.de

Received May 30, 2011

Abstract—The relationship between El-Niño/Southern Oscillation (ENSO) and the Indian monsoon is analyzed using cross-wavelet analysis and Granger causality estimation from empirical data for the period 1871–2003. In addition to the previously known negative correlation between the processes analyzed, their bidirectional coupling is detected and characteristics of its inertia and nonlinearity are estimated. The results from an analysis of variations in coupling characteristics in a moving window with a width ranging from 10 to 100 years demonstrate an alternation of different regimes of processes interaction, including intervals of almost unidirectional coupling.

Keywords: El-Niño, Southern Oscillation, Indian monsoon, climatic processes, climate change.
DOI: 10.1134/S0001433812010082

INTRODUCTION

Major climatic processes of global importance are linked to El-Niño/Southern Oscillation (ENSO) events and the Indian monsoon [1]. The strongest interannual variations in global surface temperature depend on the intensity of ENSO events. Over two-thirds of the earth's population live in monsoon-related regions (with a key role played by the Indian monsoon) [2]. An investigation into the interaction between ENSO and Indian monsoon activity is both of regional and global interest. A relationship between these processes has been reliably detected with different methods [3–11].

The increase in sea-surface temperature (SST) in the equatorial Pacific during El-Niño along with the corresponding change in convective processes, the Walker zonal circulation, the Hadley meridional circulation, and the displacement of the intertropical convergence zone is accompanied by considerable seasonal anomalies of temperature and precipitation in many regions. There are significant variations in a strong negative correlation between characteristics of the El-Niño and Indian monsoon, in particular, its noticeable decrease since the last quarter of the 20th century [1]. In addition to the analysis of coherence between the processes, an investigation of the interaction between ENSO and the Indian monsoon should involve an estimation of the strength of the impact of one process on another, i.e., quantitative estimates of directional coupling and tendencies in its variation under climate changes. In this paper such estimates are obtained by cross-wavelet analysis and Granger causality analysis, both in a linear [13] and nonlinear [14–16] version, which is used in Earth sciences more and more often (see [17–23]).

DATA

In the analysis we used monthly means of the ENSO and Indian monsoon indices for the period 1871–2003. As the ENSO index, we used the SST in the Niño3 region (5° S–5° N, 150° W–90° W)) in the Pacific Ocean from the GISST2.3 data for 1871–1996 [24] (available at http://paos.colordo.edu/research/wavelets/nino3data.asc) supplemented with data for 1997–2003 [25] (http://www.cpc.noaa.gov/data/indices/sstoi.indices), analogously to the approach available at http://atoc.colorado.edu/research/wavelets/wavelet1.html. The Indian monsoon was characterized by variations in all-India monthly rainfall [26]. The monsoon index is denoted by $x_1(t)$ and the ENSO index by $x_2(t)$.

Seasonal variations in both processes are related to a common external forcing: the annual insolation cycle. An imposed common external forcing can lead to erroneous conclusions that one process influences

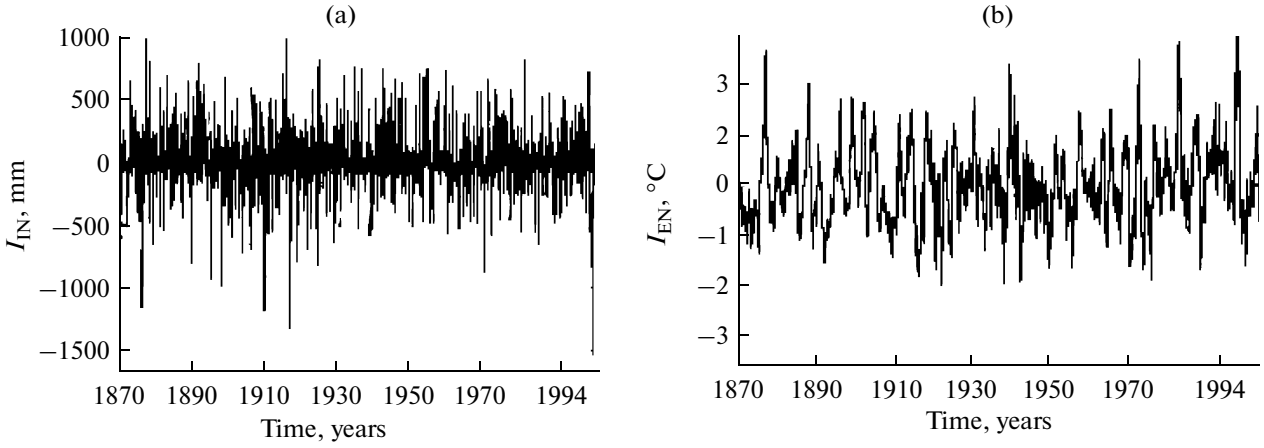

Fig. 1. Characteristics with a removed annual cycle: (a) Indian monsoon and (b) ENSO.

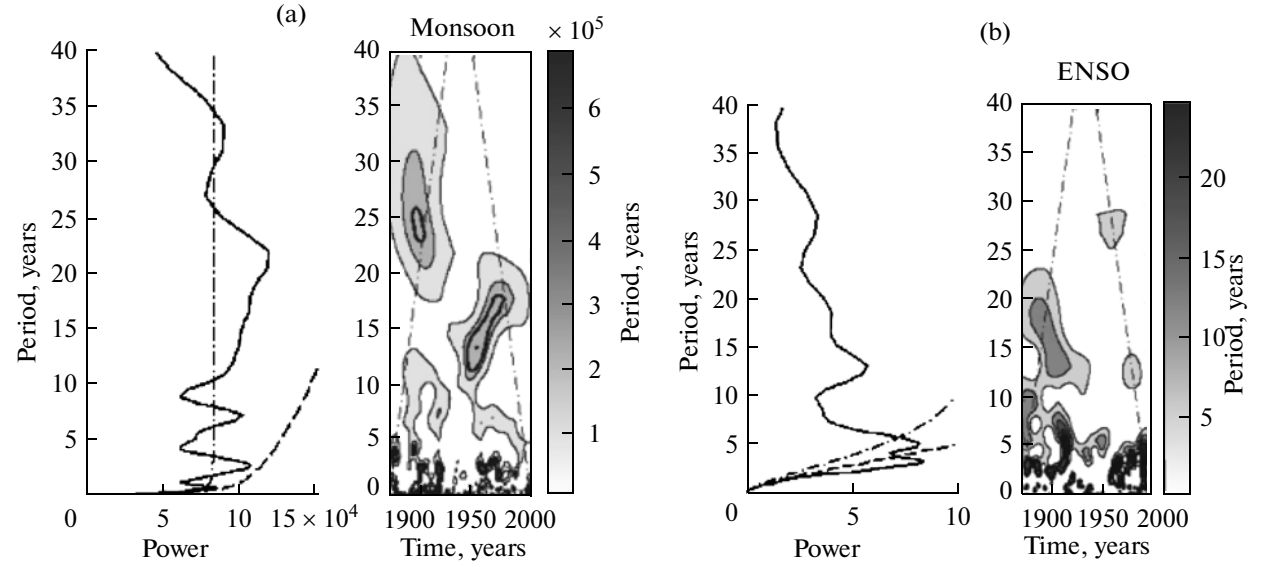

Fig. 2. (right) Local and (left) integral wavelet spectra: (a) Indian monsoon and (b) ENSO. The dotted-and-dashed lines in local spectra separate regions of edge effects, and the thick lines bound regions where the signal power is greater than expected for a "stationary red-noise model" at the significance level $p = 0.05$. In the integral spectra, the dashed lines show the 95% quantile of power for a red-noise model and the dotted-and-dashed lines indicate its mean value.

another. Therefore, to remove the seasonal variability, the annual cycle was subtracted from both time series. For this purpose, mean values of x_k (averaged over the entire 1871–2003 period) were calculated for each month, for example, January. The monthly means were then subtracted from all January values of x_k, and so on. The symbols x_1 and x_2 are retained below for the deseasonalized indices.

The time series analyzed here are shown in Fig. 1.

WAVELET AND CROSS-WAVELET ANALYSIS

Local and integral wavelet spectra of the time series analyzed are shown in Fig. 2 [27]. The largest power for the monsoon is concentrated in intra-annual variations, as is seen from the local spectrum. For ENSO, components with periods of about 3 and 5 years are noted in both the integral and local spectra.

The estimate of a cross-correlation function (CCF) for the investigated signals has a maximum absolute value of –0.22 for a 3-month time lag of ENSO relative to the monsoon. The standard deviation of the CCF estimate according to the Bartlett formula [28] is 0.025. Under the assumption of the Gaussian distribution of the CCF estimate, which is valid for the available rather long time series, one can find a 95% confidence interval: -0.22 ± 0.05. Although the absolute

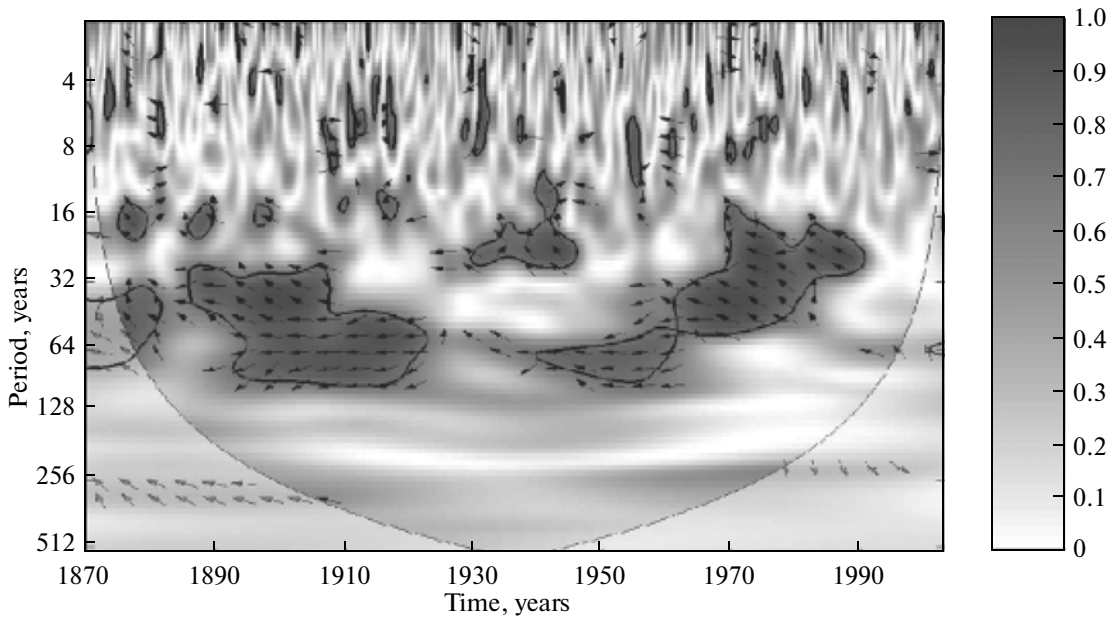

Fig. 3. Wavelet coherence between the Indian monsoon and ENSO. The solid lines separate regions of edge effects, and solid lines bound regions where the wavelet coherence differs from zero at the significance level $p = 0.05$.

value of CCF is not large, it is different from zero with very high confidence probability.

Cross-wavelet analysis (analogously, for example, to [12]) uncovers the strongest coherence between the ENSO and Indian monsoon indices on timescales ranging from 2 to 7 years (Fig. 3). In this case, along with high-coherence intervals, intervals of weakening coupling or even the absence of significant coupling between these processes are detected. Moreover, the extent of the phasing of overall antiphase mutual changes with an alternation of the driving and driven processes is varied.

ESTIMATION OF GRANGER CAUSALITY

Let there be time series from two processes $\{x_k(t)\}$, $t = 1, 2,...,N$, $k = 1, 2$, where x_k denotes variables and N is the series length. It is necessary to find out whether the process x_1 affects x_2 (the influence $1 \to 2$) and vice versa ($2 \to 1$). If an influence is found, one can find its quantitative characteristics, including estimates of inertia, nonlineariry, etc. For this purpose, the concept of Granger causality is used, the estimates of which are based on the construction of empirical models and a calculation of prediction errors of one process with and without the inclusion of another.

For a linear estimation of Granger causality [13], we first construct individual autoregressive (AR) models for $x_1(t)$ and $x_2(t)$

$$x_k(t) = A_{k,0} + \sum_{i=1}^{d_k} A_{k,i} x_k(t-i) + \xi_k(t), \quad k = 1,2, \qquad (1)$$

where d_k is a model dimension and ξ_k is Gaussian white noise. Let us denote the vector of the coefficients $\mathbf{A}_k$,I by $A_{k,i}$, $\Sigma_k^2 = \sum_{t=i_0+1}^{N} (x_k(t) - A_{k,0} - \sum_{i=1}^{d_k} A_{k,i} x_k(t-i))^2$ is the sum of the model's squared residual errors (i_0 see below). The vector $\mathbf{A}_k$ is estimated via the least-squares technique: $\hat{\mathbf{A}}_k = \arg\min_{\mathbf{A}_k} \Sigma_k^2$. Let us denote $s_k^2 = \min_{\mathbf{A}_k} \Sigma_k^2$, then an unbiased estimator of the variance of ξ_k is $\hat{\sigma}_k^2 = \dfrac{s_k^2}{N - i_0 - (d_k + 1)}$, where $d_k + 1$ is the number of estimated coefficients.

Next, a joint AR model is constructed

$$x_k(t) = a_{k,0} + \sum_{i=1}^{d_k} a_{k,i} x_k(t-i) + \sum_{i=1}^{d_{j\to k}} b_{k,i} x_j(t-i) + \eta_k(t), j, \quad k = 1,2, \quad j \neq k, \qquad (2)$$

where $d_{j\to k}$ is the dimension of an addition to the equation of one process of the data from the other process, which may be regarded as a characteristic of influence ineria, and η_k is Gaussian white noise. Analogously, $\Sigma_{k|j}^2 = \sum_{t=i_0+1}^{N} (x_k(t) - a_{k,0} + \sum_{i=1}^{d_k} a_{k,i} x_k(t-i) + \sum_{i=1}^{d_{j\to k}} b_{k,i} x_j(t-i))^2$ is the sum of mean squared prediction errors of the process x_k with x_j taken into account, where $i_0 = \max\{d_k, d_{j\to k}\}$. Let us denote a minimum value of $\Sigma_{k|j}^2$ by $s_{k|j}^2$, and the unbiased esti-

mator of the variance of residual errors by $\hat{\sigma}^2_{k|j}$. The prediction improvement of x_k with x_j taken into account characterizes the influence $j \to k$: $PI_{j\to k} = \hat{\sigma}^2_k - \hat{\sigma}^2_{k|j}$. Below we consider the normalized value $PI_{j\to k}/\hat{\sigma}^2_k$ everywhere.

To assess the statistical significance of the difference of $PI_{j\to k}$ from zero, an F-test is used [29]. Let P_k and $P_{k|j}$ denote the number of coefficients in the individual and joint models of the process x_k, respectively. For the statistically independent processes x_1 and x_2,

$$F_{j\to k} = \frac{(N - i_0 - P_{k|j})(s^2_k - s^2_{k|j})}{(P_{k|j} - P_k)s^2_{k|j}}, \quad (3)$$

is distributed according to the Fisher F-law with the number of degrees of freedom $(P_{k|j} - P_k,\ N - i_0 - P_{k|j})$. The presence of the influence $j \to k$ is inferred at the statistical significance level p, i.e., with a probability of random error no greater than p if $F_{j\to k}$ exceeds the $(1-p)$ quantile of the F distribution.

To describe nonlinearity in models, the procedure remains the same but the models are constructed with nonlinear functions, for example, individual models of the form

$$x_k(t) = f_k(x_k(t-1), x_k(t-2), \ldots, x_k(t-d_k), \mathbf{A}_k) + \xi_k(t) \quad (4)$$

and analogous joint models

$$\begin{aligned} x_k(t) = f_{k|j}(&x_k(t-1), \ldots, x_k(t-d_k),\\ &x_j(t-1), \ldots, x_j(t-d_{j\to k}), \mathbf{A}_k) + \eta_k(t), \end{aligned} \quad (5)$$

where f_k and $f_{k|j}$ are polynomials of an order L_k. It is important, however, to choose the form of nonlinear functions in a proper way. However, there is no regular procedure that would guarantee a good choice. Several studies have employed polynomials [16, 18], radial basis functions [14], or local models [15]. In what follows, low-order algebraic polynomials will be used.

To select d_k, $d_{j\to k}$ and L_k, a specific algorithm is used. For a fixed L_k, d_k should be chosen large enough for residual errors of the model to be δ-correlated. For automatization of the procedure, it is convenient to use the Schwartz information criterion [30]: d_k is chosen so as to minimize $S_k = \frac{N}{2}\ln\hat{\sigma}^2_k + \frac{\ln N}{2}P_k$. Next it is sufficient to check the AR model for adequacy. First, residual errors must be δ-correlated for the application of the F-test. Second, time realizations of the model must be close to the observed time series $x_k(t)$ in a statistical sense: the plots are similar visually, the range of probable values of the model variables contains the entire observed time series, etc. If this is the case, an individual model is satisfactory; otherwise, the value of d_k must be increased. To choose $d_{j\to k}$ for the selected d_k, one can also use the Schwartz criterion, i.e., minimize $S_{j\to k} = \frac{N}{2}\ln\hat{\sigma}^2_{k|j} + \frac{\ln N}{2}P_{k|j}$. Selecting $d_{j\to k}$, that provides a maximum value of $PI_{j\to k}$ or gives $PI_{j\to k}$ greater than zero at the minimum significance level p is more suitable for finding the coupling between processes. In practice, the two criteria more often give similar results. Next, the adequacy of the joint AR model is checked as was indicated above and, if necessary, the sample value of $d_{j\to k}$ is varied. The choice of L_k is made according to the Schwartz criterion or to the most significant $PI_{j\to k}$. The sampling values of d_k, $d_{j\to k}$, L_k should be sought within such a range that the number of coefficients in any fitted AR model is far less than N. By a rough estimate, it may not exceed $\sqrt{N}$, i.e., approximately 40 in the case analyzed.

The estimates were first calculated for the entire period 1871–2003; then an analysis was performed in a moving window of width from 10 to 100 years.

INDIVIDUAL MODELS

For linear models, the number of coefficients is $P_k = d_k + 1$, so that d_k can be increased to 39 in constructing a model from data for the entire 1871–2003 period. For quadratic models, $P_k = \frac{(d_k+1)(d_k+2)}{2}$, so that even d_k cannot not be greater than 7. For $L_k = 3$, there must be $d_k \le 4$; for $L_k = 4$ $d_k \le 3$; and so on.

For the Indian monsoon, the model is optimal at $d_1 = 1$ for any L_1 (Fig. 4a). The Schwartz criterion has a smaller value for the linear model. Thus, the linear model with $d_1 = 1$ is optimal. It gives a prediction error with variance $\hat{\sigma}^2_1/\mathrm{var}[x_1] = 0.98$, where $\mathrm{var}[x_1]$ is the empirical variance of x_1; that is, the model explains just 2% of the variance of x_1.

For ENSO, nearly the same value of the Schwartz criterion is obtained for two values of the dimension of a linear model $d_2 = 1$ and $d_2 = 5$ (Fig. 4b). As for the estimate of the cross-correlation function of residual errors, it is significantly different from the delta function at $d_2 = 1$ and not significantly at $d_2 = 5$ (not shown). For $L_2 > 1$, an optimal version is achieved at $d_2 = 1$; however, to ensure the uncorrelatedness of residuals, d_2 must be increased to 5. The Schwartz criterion for linear models is lower than for the nonlinear ones. On the basis of these results, the linear model with $d_2 = 5$ should be considered optimal. The normalized variance of its prediction error is $\hat{\sigma}^2_2/\mathrm{var}[x_2] = 0.18$.

An analysis of residual prediction errors of the optimal models of both processes demonstrates their delta correlatedness. Moreover, the distribution of residuals is close to Gaussian distribution. Thus, the F-test is suitable for estimating the Granger causality.

INFLUENCE OF ENSO ON THE MONSOON

In constructing models for the monsoon with ENSO impact at different L_1, $d_1 = 1$ is always used by taking into account the results given in Fig. 4a. For $L_1 = 1$ and $L_1 = 3$, $d_{2\to1} = 1$ is optimal according to the Schwartz criterion (Fig. 5a). Of them, the linear model yields the lower Schwartz criterion. However, the model with $L_1 = 3$ gives the largest and most significant prediction improvement, and this more complicated model should be considered optimal for an analysis of coupling. The prediction improvement in this case is $PI_{2\to1}/\hat{\sigma}_1^2 = 0.028$, i.e., approximately 3% of the variance of all the factors unexplained by the individual model. This influence is statistically significant.

The choice of $d_{2\to1} = 1$ means inertialess influence. Although the linear and nonlinear models produce similar results, the larger statistical significance of the inference about influence at $L_1 = 3$ allows us to conclude that there are signs of the nonlinear influence of ENSO on the monsoon. The model with $L_1 = 3$ is

$$x_1(t) = a_{1,1}x_1(t-1) + b_{1,1}x_2(t-1) + c_{1,1}x_1^2(t-1)x_2(t-1) + c_{1,2}x_2^3(t-1) + \eta_1(t), \quad (6)$$

where $\sigma_{\eta_1}^2 = 5.86 \times 10^4$ mm^2 and estimates of the coefficients and of their standard deviations [29] are $a_{1,1} = 0.082 \pm 0.037$, $b_{1,1} = -46.7 \pm 11.2$ mm^{-1} K^{-1}, $c_{1,1} = (-3.5 \pm 0.76) \times 10^{-4}$ mm^{-1} K^{-2}, $c_{1,2} = 15.3 \pm 3.8$ mm K^{-3}. Only those terms in the model for which the estimates of coefficients are different from zero, at least at the significance level 0.05, i.e., by more than twice the estimate of standard deviation, are shown. The linear coupling coefficient $b_{1,1}$ is negative, which corresponds to the negative correlation between the signals.

INFLUENCE OF THE MONSOON ON ENSO

A joint model for ENSO is optimal at $L_2 = 1$ and $d_{1\to2} = 3$ (Fig. 5b). It gives the most significant prediction improvement, which is $PI_{1\to2}/\hat{\sigma}_2^2 = 0.024$ and above zero at the significance level $p < 5 \times 10^{-9}$. This model has the form

$$x_2(t) = a_{2,1}x_2(t-1) + a_{2,5}x_2(t-5) + b_{2,1}x_1(t-1) + b_{2,2}x_1(t-2) + b_{2,3}x_1(t-3) + \eta_2(t), \quad (7)$$

where $\sigma_{\eta_2}^2 = 0.11$ K^2, $a_{2,1} = 0.92 \pm 0.02$, $a_{2,5} = -0.084 \pm 0.025$, $b_{2,1} = (-1.48 \pm 0.34) \times 10^{-4}$ mm^{-1} K,$^{-1}$ K, $b_{2,2} = (-1.00 \pm 0.35) \times 10^{-4}$ mm^{-1} K, and^{-1} K, $b_{2,3} = (-1.08 \pm 0.35) \times \times 10^{-4}$ mm^{-1} K. The influence is inertial: $d_{1\to2} = 3$; i.e., the behavior of the ENSO index depends on the values of the monsoon index for the three previous months. The coupling coefficients are negative, which means the anticorrelation of the variables $x_1(t)$ and $x_2(t)$. All the three coupling coefficients have similar values; i.e., the total contribution of the monsoon index $b_{2,1}x_1(t-1) + b_{2,2}x_1(t-2) + b_{2,3}x_1(t-3)$ to the equation for ENSO is approximately proportional to its average value over three months. No signs of nonlinearity of this influence are detected.

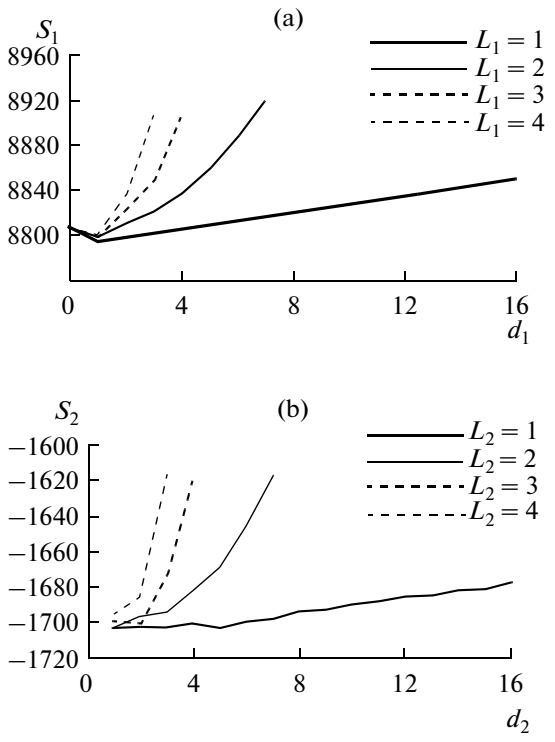

Fig. 4. Schwarz criterion for individual AR models: (a) monsoon and (b) ENSO.

It can be seen in Figs. 5b, 5d, and 5f that there is an additional prediction improvement at $d_{1\to2} = 10$ with a contribution from the values of the monsoon index $x_1(t-9)$ and $x_1(t-10)$. Here the coefficients $b_{2,9}$ and $b_{2,10}$ are positive. However, they are significantly different from zero only at the pointwise level $p = 0.02$. Because these are only two of the seven additionally introduced coupling coefficients, the common level of significance of the inference about their difference from zero can be estimated to be $0.02 \times 7 = 0.14$; i.e., the inference is not very reliable. Thus we can only suggest that weak signs of an additional delayed impact of the monsoon on ENSO have been detected.

ANALYSIS OF THE ADEQUACY OF AN OPTIMAL JOINT MODEL

The structure of time realizations of an optimal model ($L_1 = 3, d_1 = 1, d_{2\to1} = 1, L_2 = 1, d_2 = 5, d_{1\to2} = 3$) is visually similar to the structure of the original series (Fig. 6a). For a quantitative testing, an ensemble of model realizations was generated under identical initial conditions and the 95% range of model values was determined. Then 95% of observed values of the mon-

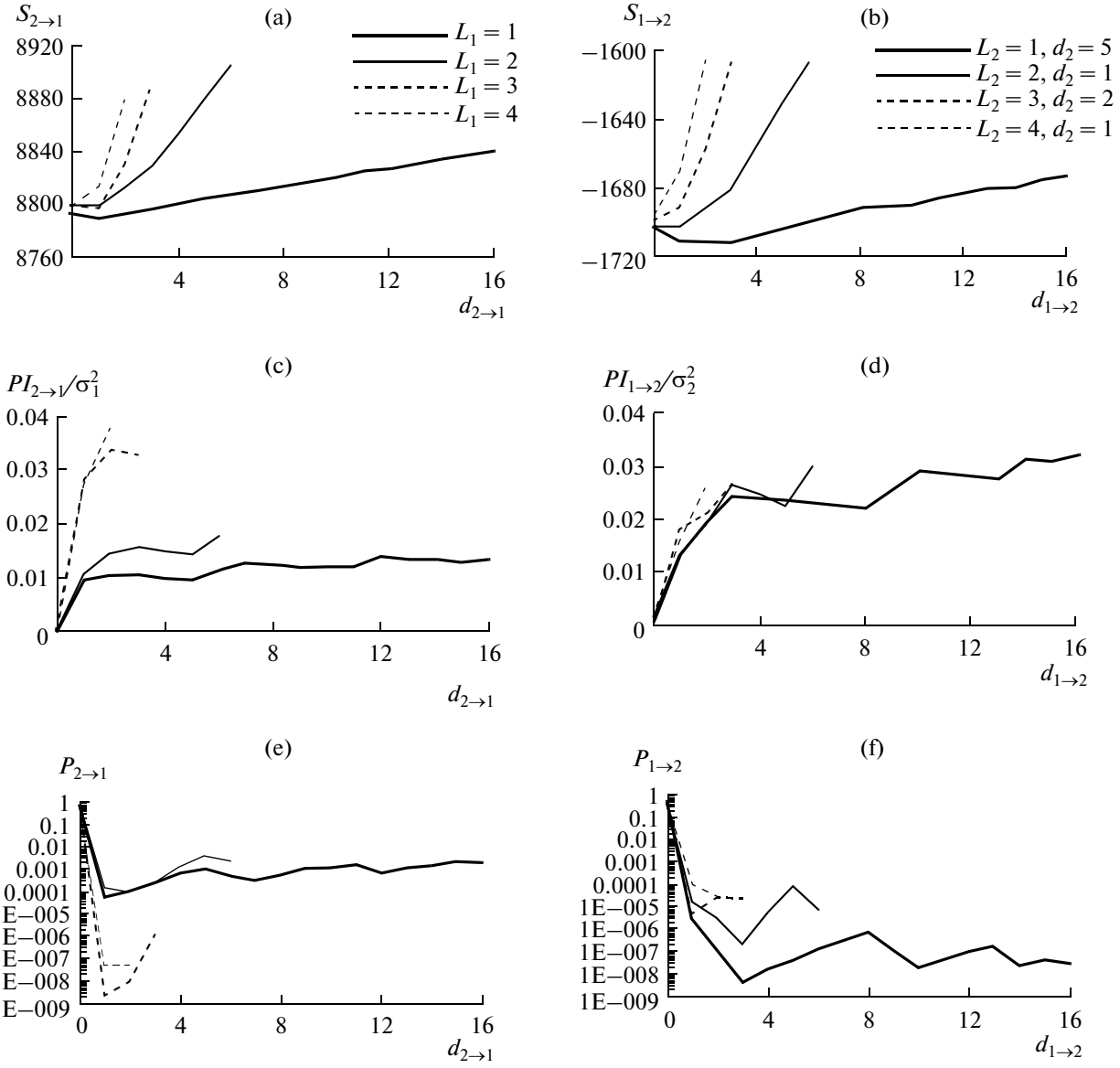

Fig. 5. Schwarz criterion: (a) monsoon and (b) ENSO. Prediction improvement: (c) monsoon and (d) ENSO. Significance level of the difference of prediction from zero: (e) monsoon and (f) ENSO.

soon and ENSO indices lie within this range (Fig. 6b), thus confirming the model's adequacy. The cross correlation between residual prediction errors for the monsoon and ENSO is zero; therefore, the coupling occurs not through a common external forcing.

ANALYSIS OF THE COUPLING IN MOVING WINDOWS

An analysis of characteristics of the coupling between ENSO and the Indian monsoon was also carried out in a moving time window, i.e., in the intervals $[T-W, T]$, where W is the window length and T is the coordinate of the window endpoint. For a fixed W (which was varied within the range from 10 to 100 years with a step of 10 years), computations were made for T from $1870 + W$ to 2003. When several time windows are analyzed, the significance level of the inference about the presence of coupling is more difficult to estimate (with a correction for a multiplele character of the test). Namely, according to the procedure described above, the estimates of prediction improvements and of the significance level of the inference about coupling are calculated separately for each time series. This is a so-called pointwise significance level, i.e., the probability of a random error for an individual window. The probability of erroneously making an inference about coupling that is significant at the pointwise level p for at least one of the M nonoverlapping windows is $p \cdot M$ according to the rule of summa-

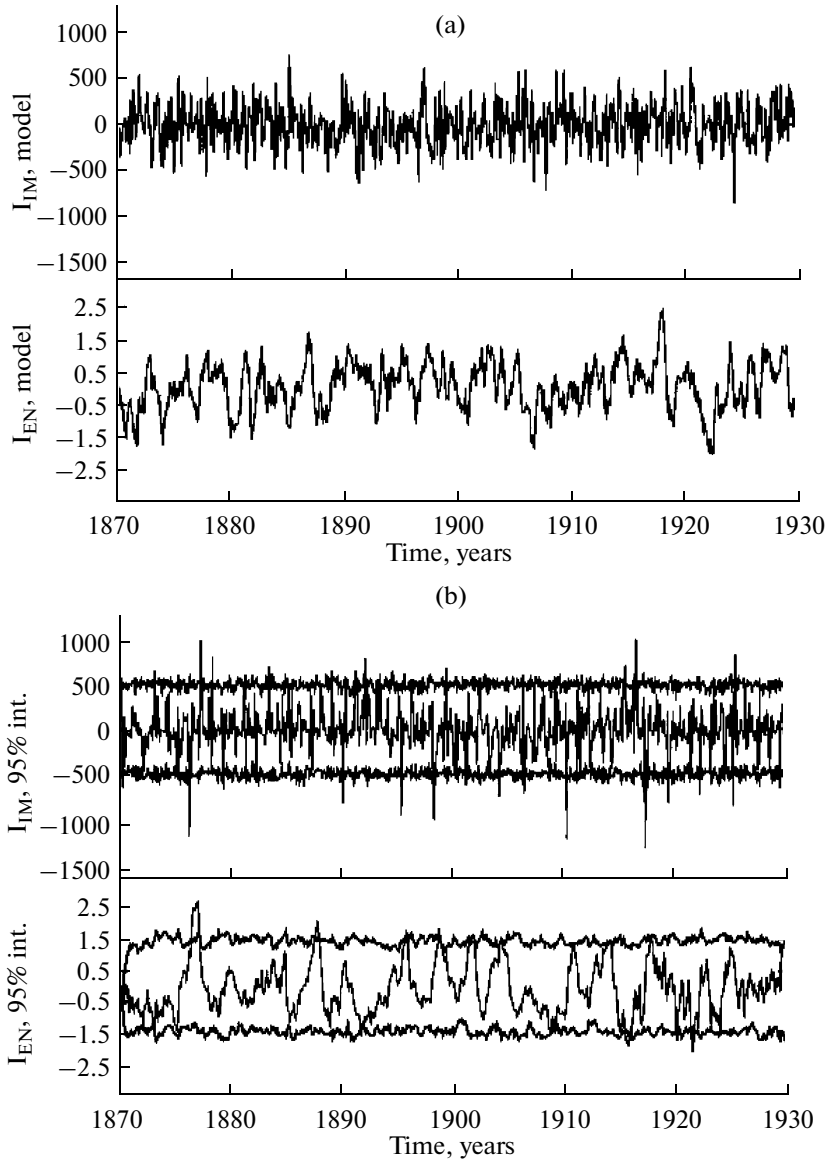

Fig. 6. Behavior of the optimal AR model: (a) time realizations for monsoon characteristics (top) and for ENSO (bottom); (b) the 95% range of model realizations and observed original time series.

tion of probabilities of combining the independent events (for small $p \cdot M$). Thus, to make a final inference about coupling in one of the analyzed windows at the significance level p, it is necessary that the pointwise level for this window should be p/M, where $1/M$ is called the Bonferroni correction. The dashed lines in Figs. 7 and 8 show $p = 0.05/(N/W)$, where N/W is the number of nonoverlapping windows: if the pointwise significance level for a particular window is lower than this value, the presence of coupling is inferred at a significance level lower than 0.05 for that window.

Estimates of the ENSO impact on the monsoon are shown in Fig. 7 for an optimal nonlinear model at $d_1 = d_{2\to1} = 1$, $L_1 = 3$ with a window length of 30 and 100 years. The 100-year window gives highly significant results for any T. The long-term tendency is that the influence of ENSO on the monsoon increases slightly at the beginning of the period analyzed, reaches a maximum, and then weakens. The period of the weakening influence is longer than the period when the influence increases. When the window length is decreased, the significance of results falls but the time resolution grows. For example, the 30-year window shows the existence of coupling for $1910 \le T \le 1930$ and $1975 \le T \le 1985$, i.e., over intervals of 1880–1930 and 1945–1985. For a smaller window, the nonlinear model becomes very cumbersome and produces less significant results. In general it may be concluded that the impact of ENSO on the monsoon was weak before 1880, in 1930–1945, and after 1985.

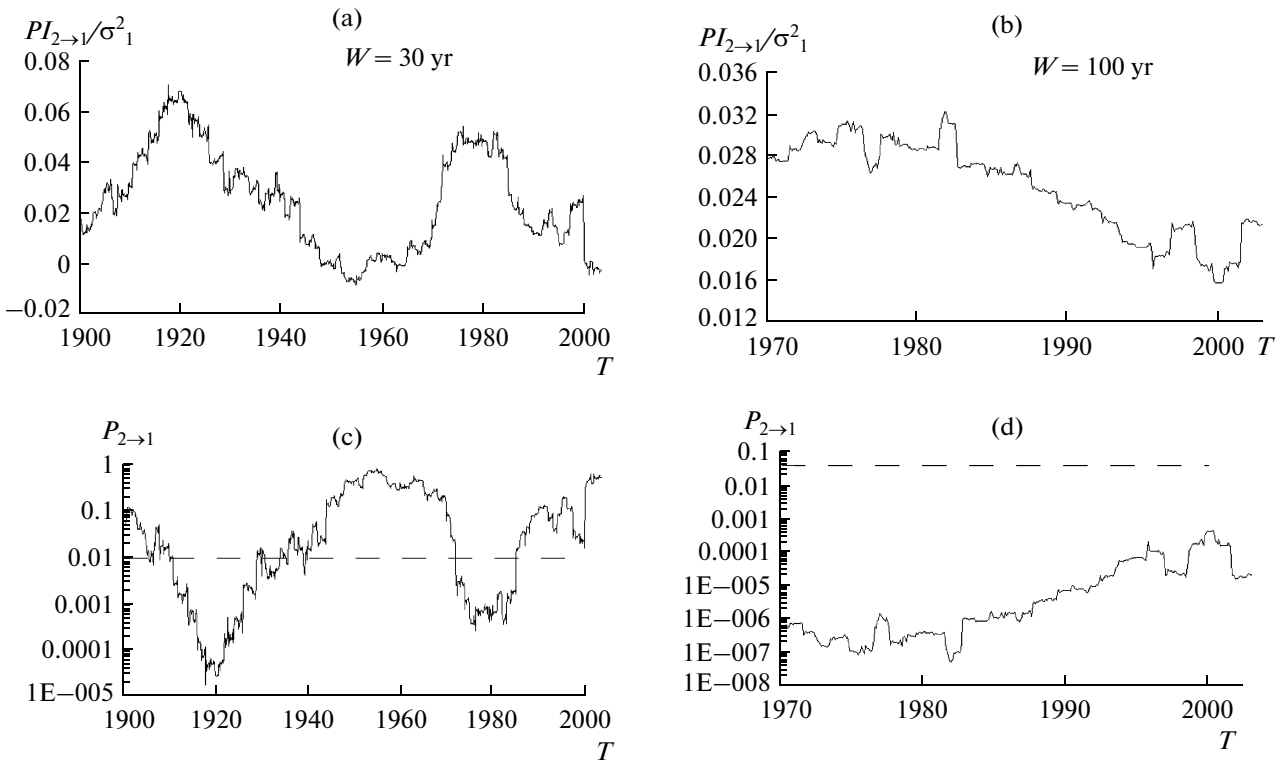

Fig. 7. Estimates of the ENSO influence on the monsoon in a moving window $[T-W, T]$ versus the coordinate of the window endpoint T: (a) prediction improvement for a 30-year window, (b) prediction improvement for a 100-year window, (c) significance level for a 30-year window, and (d) significance level for a 100-year window. The dashed lines show the Bonferroni-corrected pointwise significance levels corresponding to $p = 0.05$.

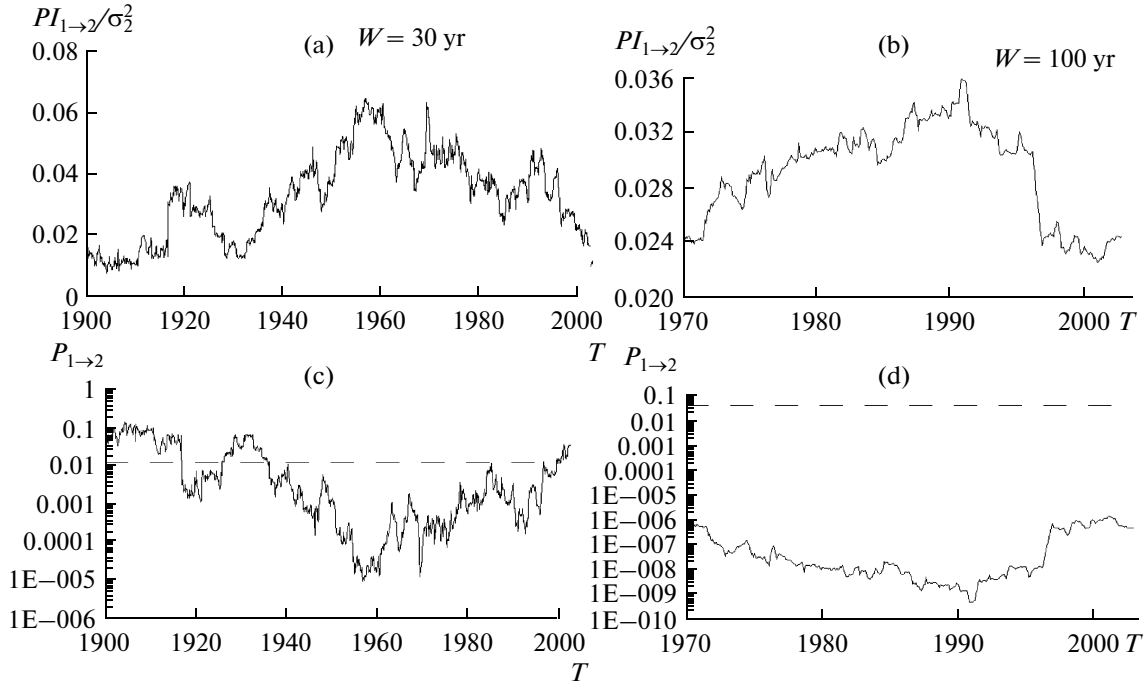

Fig. 8. Estimates of the monsoon influence on ENSO in a moving window $[T-W, T]$ versus the coordinate of the window endpoint T: (a) prediction improvement for a 30-year window, (b) prediction improvement for a 100-year window, (c) significance level for a 30-year window, and (d) significance level for a 100-year window. The dashed lines show the Bonferroni-corrected pointwise significance levels corresponding to $p = 0.05$.

For a 100-year time window, the significant influence of the monsoon on ENSO (Fig. 8) is detected for any T (Fig. 8). The long-term tendency is the same as that in the ENSO influence on the monsoon, but a decrease in the influence of the monsoon on ENSO began somewhat later (the maximum of dependence is nearer 2003). For a 30-year window, the significant influence of the monsoon on ENSO is detected for $1917 \le T \le 1927$ and, especially, for $1935 \le T \le 2000$, i.e., actually over the entire time series. For a smaller window length, the significant influence is detected only in the interval 1930–1960 (20-year window) or it is not detected at all (10-year window). In general it may be concluded that the impact of the monsoon on ENSO is more steadily detected than that of ENSO on the monsoon. It is absent only before 1890 and most significant in 1930–1950. The intervals of the strongest ENSO-to-monsoon and monsoon-to-ENSO coupling do not coincide in time but follow each other.

The coupling detected between the processes is approximately symmetric: the normalized prediction improvement in both directions is 2–3% in the analysis for the entire 1871–2003 interval and has a maximum 7% when a 30-year window is used.

Intervals of 1 : 1 synchronization (the phase difference between the two signals $\phi_1 - \phi_2$ is approximately constant) between the investigated processes were found in [9]: 1886–1908 corresponds to a strong influence of ENSO on the monsoon from our results, and 1964–1980 acts analogously. The synchronization of 1 : 2 ($\phi_1 - 2\phi_2$ is approximately constant) was detected for 1908–1921 (a predominant monsoon influence on ENSO), 1935–1943 (the largest influence of the monsoon on ENSO and no influence of ENSO on the monsoon), and 1981–1991 (a predominant influence of the monsoon on ENSO). Thus, it can be noted that 1 : 1 synchronization coincides with intervals when ENSO has a stronger influence on the monsoon while 1 : 2 synchronization corresponds to a predominant influence of the monsoon on ENSO.

CONCLUSIONS

Based on Granger causality and cross-wavelet analysis, we have obtained new more detailed characteristics of the interaction between the investigated climatic processes in comparison with previously known results on their anticorrelation [3] and intervals of phase synchrony [9]. The bidirectional coupling between ENSO and the Indian monsoon is detected with high confidence. The impact of ENSO on the monsoon is inertia-free and nonlinear. The impact of the monsoon on ENSO is linear with a 3-month lag time. The coupling is almost symmetric: the prediction improvement is 2–3% for both directions.

An analysis in moving windows reveals the alternating character of the coupling between ENSO and the Indian monsoon. The influence that the monsoon exerts on ENSO increases from the late 19th century to about 1930–1950, when it is maximal. It weakens in the last decade of the 20th century. The inverse influence is maximal about 1890–1920, slightly noticeable in 1950–1980, and not detected at all between these intervals and after 1980.

ACKNOWLEDGMENTS

This study was supported by the Russian Foundation for Basic Research, (project no. 11-05-01139-a), the Russian Ministry of Education and Science, and programs of the Russian Academy of Sciences.

REFERENCES

1. *Climate Change 2007: The Physical Science Basis,* Ed. by S. Solomon, D. Qin, M. Manning, et al., (Cambridge University Press, Cambridge, 2007).
2. T. Zhou, L. Zhang, and H. Li, "Changes in Global Land Monsoon Area and Total Rainfall Accumulation over the Last Half Century," Geophys. Rev. Lett. **35**, L16707 (2008). doi: 10.1029/2008GL034881
3. E. W. Bliss and G. T. Walker, "World Weather V," Mem. R. Meteorol. Soc. **4** (36), 53–84 (1932).
4. R. H. Kripalani and A. Kulkarni, "Rainfall Variability over Southeast Asia: Connections with Indian Monsoon and ENSO Extremes: New Perspectives," Int. J. Climatol. **17** (11), 1155–1168 (1997).
5. K. K. Kumar, B. Rajagopalan, and A. M. Cane, "On the Weakening Relationship between the Indian Monsoon and ENSO," Science **284** (5423), 2156–2159 (1999).
6. V. Krishnamurthy and B. N. Goswami, "Indian Monsoon–ENSO Relationship on Interdecadal Timescale," J. Clim. **13** (3), 579–595 (2000).
7. R. H. Kripalani and A. Kulkarni, "Monsoon Rainfall Variations and Teleconnections over South and East Asia," Int. J. Climatol. **21** (5), 603–616 (2001).
8. S. Sarkar, R. P. Singh, and M. Kafatos, "Further Evidences for the Weakening Relationship of Indian Rainfall and ENSO over India," Geophys. Rev. Lett. **31**, L13209 (2004). doi: 10.1029/2004GL020259
9. D. Maraun and J. Kurths, "Epochs of Phase Coherence between El Nino/Southern Oscillation and Indian Monsoon," Geophys. Rev. Lett. **32**, L15709 (2005). doi: 10.1029/2005GL023225
10. L. Zubair and C. F. Ropelewski, "The Strengthening Relationship between ENSO and Northeast Monsoon Rainfall Over Sri Lanka and Southern India," J. Clim. **19** (8), 1567–1575 (2006).
11. S.-Y. Yim, J. -G. Jhun, and S. -W. Yeh, "Decadal Change in the Relationship between East Asian-Western North Pacific Summer Monsoons and ENSO in the Mid-1990s," Geophys. Rev. Lett. **35**, L20711 (2008). doi: 10.1029/2008GL035751
12. S. Jevrejeva, J. C. Moore, and A. Grinsted, "Influence of the Arctic Oscillation and El Nino-Southern Oscillation (ENSO) on Ice Conditions in the Baltic Sea: The Wavelet Approach," J. Geophys. Res. **108** (D21), 4677 (2003). doi: 10.1029/2003jd003417

13. C. W. J. Granger, "Investigating Causal Relations by Econometric Models and Cross-Spectral Methods," Econometrica **37** (3), 424–438 (1969).
14. N. Ancona, D. Marinazzo, and S. Stramaglia, "Radial Basis Function Approach to Nonlinear Granger Causality of Time Series," Phys. Rev. E **70** 056221 (2004). doi: 10.1103/PhysRevE.70.056221
15. U. Feldmann and J. Bhattacharya, "Predictability Improvement as an Asymmetrical Measure of Interdependence in Bivariate Time Series," Int. J. Bifurc. Chaos **14** (2), 505–514 (2004).
16. K. Ishiguro, N. Otsu, M. Lungarella, et al., "Detecting Direction of Causal Interactions Between Dynamically Coupled Signals," Phys. Rev. E: **77** (3), 026216 (2008).
17. W. Wang, B. T. Anderson, R. K. Kaufmann, et al., "The Relation between the North Atlantic Oscillation and SSTs in North Atlantic Basin," J. Clim. **17** (24), 4752–4759 (2004).
18. I. I. Mokhov and D. A. Smirnov, "El-Niño-Southern Oscillation Drives North Atlantic Oscillation as Revealed with Nonlinear Technique from Climatic Indices," Geophys. Rev. Lett. **33**, L03708 (2006a). doi: 10.1029/2005GL024557
19. I. I. Mokhov and D. A. Smirnov, "Study of the Mutual Influence of the El-Niño–Southern Oscillation Processes and the North Atlantic and Arctic Oscillations," Izv. Atmos. Okean. Phys. **42** (5), 598–614 (2006).
20. T. J. Mosedale, D. B. Stephenson, M. Collins, et al., "Granger Causality of Coupled Climate Processes: Ocean Feedback on the North Atlantic Oscillation," J. Clim. **19** (7), 1182–1194 (2006).
21. I. I. Mokhov and D. A. Smirnov, "Diagnostics of a Cause–Effect Relation between Solar Activity and the Earth's Global Surface Temperature," Izv. Atmos. Okean. Phys. **44** (3), 263–272 (2008).
22. I. I. Mokhov, D. A. Smirnov, P. I. Nakonechny, et al., "Assessment of the Mutual Effect of El-Niño–Southern Oscillation and Indian Monsoon," in *Modern Problems of Oceanic and Atmospheric Dynamics*, Ed. by A. V. Frolov and Yu. D. Resnyanskii (Triada LTD, Moscow, 2010), pp. 251–267 [in Russian].
23. I. I. Mokhov, D. A. Smirnov, P. I. Nakonechny, et al., "Alternating Mutual Influence of El-Niño/Southern Oscillation and Indian Monsoon," Geophys. Rev. Lett. (2010). doi: 10.1029/2010Gl045932
24. N. A. Rayner, D. E. Parker, E. B. Horton, et al., "Global Analyses of Sea Surface Temperature, Sea Ice, and Night Marine Air Temperature since the Late Nineteenth Century," J. Geophys. Res. **108** (D14) (2003). doi: 10.1029/2002Jd002670
25. R. W. Reynolds and T. M. Smith, "Improved Global Sea Surface Temperature Analyses," J. Clim. **7** (6), 929–948 (1994).
26. D. A. Mooley and B. Parthasarathy, "Fluctuations in All-India Summer Monsoon Rainfall during 1871–1978," Clim. Change **6** (3), 287–301 (1984).
27. C. Torrence and G. P. Compo, "A Practical Guide to Wavelet Analysis," Bull. Am. Meteorol. Soc. **79** (1), 61–78 (1998).
28. M. S. Bartlett, *An Introduction to Stochastic Processes* (Cambridge Univ. Press, Cambridge, 1978).
29. G. A. F. Seber, *Linear Regression Analysis* (Wiley, New York, 1977).
30. G. Schwartz, "Estimating the Dimension of a Model," Ann. Stat. **6** (2), 461–464 (1978).
31. A. Pikovsky, M. Rosenblum, and J. Kurths, *Synchronization. A Universal Concept in Nonlinear Sciences* (Gambridge Univ. Press, Cambridge, 2001).